Surface Science 635 (2015) 94–98

Contents lists available at ScienceDirect

Surface Science

journal homepage: www.elsevier.com/locate/susc

Magic C_{60} islands forming due to moiré interference between islands and substrate

D.A. Olyanich [a,b], V.V. Mararov [a], T.V. Utas [a,b], O.A. Utas [a,b], D.V. Gruznev [a,b], A.V. Zotov [a,b,c], A.A. Saranin [a,b,*]

[a] Institute of Automation and Control Processes, 5 Radio Street, 690041 Vladivostok, Russia
[b] School of Natural Sciences, Far Eastern Federal University, 690950 Vladivostok, Russia
[c] Department of Electronics, Vladivostok State University of Economics and Service, 690600 Vladivostok, Russia

ARTICLE INFO

Article history:
Received 16 November 2014
Accepted 7 January 2015
Available online 15 January 2015

Keywords:
Atom–solid interactions
Silicon
Fullerene
Self-assembly
Scanning tunneling microscopy

ABSTRACT

Recently proposed mechanism for self-organized formation of magic islands [Nat.Comm. 4(2013)1679] has received a new experimental confirmation. According to this mechanism, self-assembly is mediated by the moiré interference between an island and underlying substrate lattice. It was first detected at C_{60} island growth on In-adsorbed Si(111)$\sqrt{3}\times\sqrt{3}$-Au surface. Changing In adsorbate for Tl results in lowering the corrugations of the surface potential relief due to a greater surface metallization. This allows formation of the C_{60} arrays with novel moiré pattern. As a result, a new set of magic C_{60} islands is formed on Tl-adsorbed Au/Si(111) surface differing from that observed on In-adsorbed surface. For example, the 19-C_{60} magic island which has a non-compact boomerang shape on In-adsorbed Au/Si(111) surfaces adopts a shape of a regular hexagon on Tl-adsorbed surface.

1. Introduction

Arrays of atomic clusters on solid surfaces constitute a specific class of low-dimensional materials with intriguing structures, properties and mechanism of their self-assembly. Bearing in mind that cluster properties are size-dependent, there is a strong demand for finding the ways for fabricating monodispersed cluster arrays. Research activity in this field has resulted in developing the concept of surface magic clusters, i.e., the clusters exhibiting enhanced stability at selected (magic) sizes on a particular surface [1]. A number of vivid examples for self-assembled formation of magic clusters have been obtained with Group-III elements (Al [2–6], Ga [7–11], In [12–15], and Tl [16–19]) and some other elements outside of this group (e.g., Pb [20], Ag [21–24], Na [25–28], Au [29], Cu [30,31], Mn [32–35], Co [36,37]) adsorbed onto Si(111) surface. All the known magic clusters have been found to contain about a dozen atoms. Question arises if it is possible to propagate the magic cluster size to the mesoscopic range of dozens, hundreds or even thousands of atoms. Apparently, this could hardly be achieved using usual approach where magic clusters are formed via self-assembly of separate atoms, since the energy gain at typical magic cluster sizes is actually not great, hence magicity effects would smear with growing number of atoms. Possible solution is to use molecules instead of atoms as building blocks for fabrication of the large magic clusters. Recently, we have demonstrated the validity of such an approach with C_{60} fullerenes adsorbed on In-adsorbed Au/Si(111) surface [38]. It has been found that magic islands each containing 37 C_{60} (i.e., exactly 2220 carbon atoms) can constitute up to 80% of all the islands. The size selection in this case has been recognized to be mediated by the moiré interference between a growing C_{60} island with underlying surface lattice, which essentially maps out the adsorption-energy landscape of a C_{60} in different adsorption sites, hence dictates the probability for the attachment (detachment) of C_{60} to (from) an island periphery [38]. Disclosed self-assembly mechanism is based solely on the appropriate lattice matching of a growing layer and a substrate, hence seems to be rather universal and, in principle, can occur in many very different systems. However, up to now it has been detected only in the reported case of C_{60} growth on (Au, In)/Si(111) surface [38], though effects of the moiré interference on the film growth have recently been considered for a number of systems (e.g., for the growth of Pb quantum islands on Si(111) [39] and Ag nanopucks on them [40] or C_{60} monolayers on Pb(111) [41])

The goal of the present study was to look for other examples of C_{60} magic island formation via the same moiré mediated mechanism, to see which other kinds of magic islands can be formed and to elucidate which features of the surface relief are essential for controlling the size and shape of magic clusters. In the present work, we have changed the In-adsorbed Au/Si(111) surface by the Tl-adsorbed Au/Si(111) one. The surfaces have similar but not identical structures [42]. On the Tl-adsorbed Au/Si(111) surface, C_{60} arrays with a new type of azimuthal orientation are formed which results in developing a new moiré pattern. This, in turn, leads to self-assembly of magic clusters of a new

* Corresponding author.
E-mail address: saranin@iacp.dvo.ru (A.A. Saranin).

http://dx.doi.org/10.1016/j.susc.2015.01.003
0039-6028/

shape and size. Molecular dynamics simulations have revealed that the observed new features are associated with the diminished corrugations of the surface potential relief.

2. Experimental details

Our experiments were performed with a variable-temperature Omicron VT-STM operating in an ultrahigh vacuum (~2.0×10^{-10} Torr). Atomically-clean Si(111)7 × 7 surfaces were prepared in situ by flashing to 1280 °C after the samples were first outgassed at 600 °C for several hours. Gold was deposited from an Au-wrapped tungsten filament, thallium from Ta crucible and C_{60} fullerenes from a resistively heated Mo crucible. To prepare the Tl-modified Si(111)$\sqrt{3} \times \sqrt{3}$-Au surface, the Si(111)$\sqrt{3} \times \sqrt{3}$-Au surface [43] was first formed by Au deposition onto Si(111)7 × 7 surface held at 600 °C and then ~0.5 ML of Tl was deposited onto this surface held at room temperature followed by brief (~10 s) annealing at ~350 °C. The resultant surface was highly-ordered and homogeneous being free of domain walls, characteristic of the pristine Si(111)$\sqrt{3} \times \sqrt{3}$-Au surface [43]. It preserves the atomic arrangement of the $\sqrt{3} \times \sqrt{3}$-Au phase and contains ~0.20 ML of Tl left after high-temperature treatment as a 2D gas of adatoms [42].

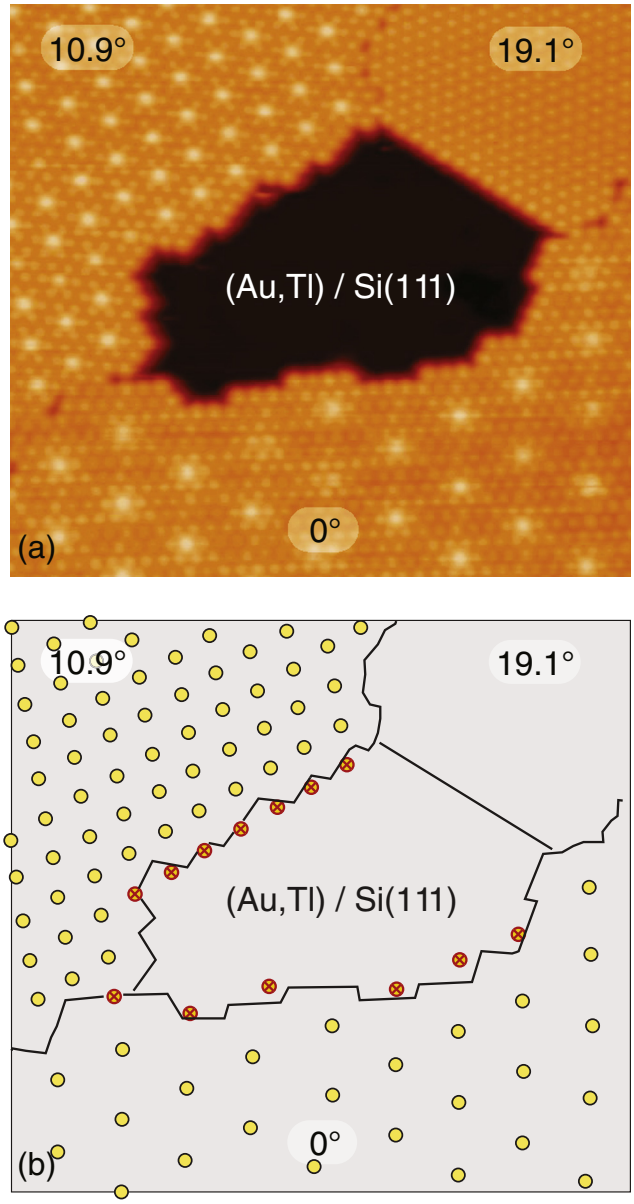

Fig. 1. (a) 380 × 380 Å^2 STM image of the Tl-adsorbed Si(111)$\sqrt{3} \times \sqrt{3}$-Au surface after RT adsorption of C_{60} fullerenes showing occurrence of the three types of C_{60} arrays differing by asimuthal orientations which surround the region of a bare (Au, Tl)/Si(111) surface. The angle which C_{60} rows make with the main crystallographic directions of the Si(111) surface, 0°, 19.1° and 10.9°, is indicated for each array. (b) Schematic diagram (a) illustrating that the shape of the edge of the growing C_{60} arrays is controlled by the moiré patterns developed in the arrays. The bright fullerenes within the arrays are shown by yellow circles, the hypothetical locations where the bright fullerenes would appear on a bare surface according to the expanding moiré patterns are shown by crossed red circles. (For interpretation of the references to color in this figure legend, the reader is referred to the web version of this article.)

3. Results and discussion

Upon deposition onto the Tl-adsorbed Si(111)$\sqrt{3} \times \sqrt{3}$-Au surface, C_{60} fullerenes self-assemble into the close packed hexagonal arrays. Three types of arrays are formed differing by their orientation with respect to the underlying substrate. In the arrays of the first type (to be called hereafter as the 0°-rotated arrays), C_{60} rows are aligned along the main crystallographic directions of the Si(111) surface, $\langle 10\bar{1} \rangle$. In the arrays of the second type (the 19.1°-rotated arrays), the C_{60} rows make an angle of 19.1° with the main crystallographic directions. In the arrays of the third type (the 10.9°-rotated arrays), this angle equals 10.9°. The 0°-rotated arrays dominate at low temperatures, the 19.1°-rotated arrays start to prevail at relatively high temperatures, fraction of the 10.9°-rotated arrays constitutes typically not more than ~3% at all temperatures. For example, 0°-, 19.1°- and 10.9°-rotated arrays occupy the area fractions of 87%, 11.5% and 1.5%, respectively, at 265 K; 75%, 22.5% and 2.5%, respectively at 300 K and 48%, 50% and 2.0%, respectively at 400 K. Fig. 1a shows the surface region where C_{60} domains of all the three types surround the patch of a bare Si(111)$\sqrt{3} \times \sqrt{3}$-(Au, Tl) surface.

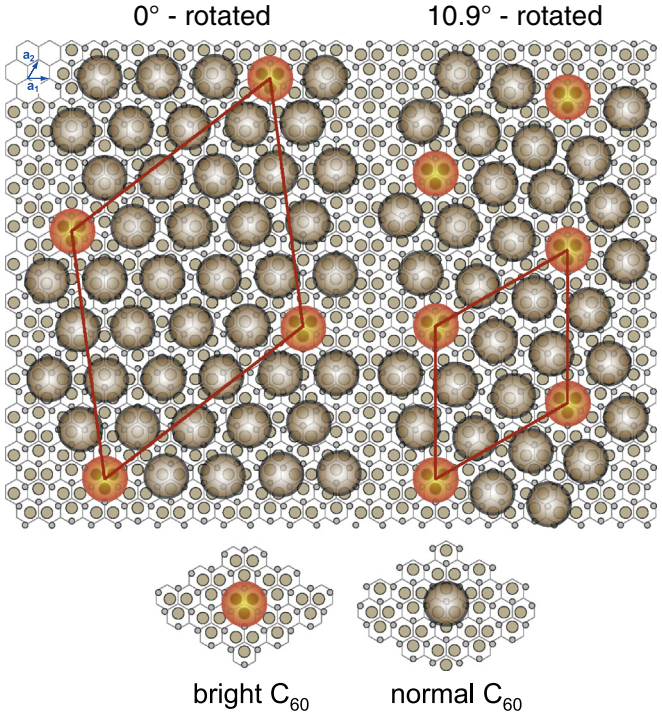

Fig. 2. Schematic diagram showing close-packed 0°-rotated (left panel) and 10/9°-rotated (right panel) C_{60} arrays superposed onto the ideal Si(111)$\sqrt{3} \times \sqrt{3}$-Au surface. Bright fullerenes shown by red-yellow circles are those located directly above the Au trimers (shown my middle-sized light gray circles). The other ("normal") fullerenes shown by large gray circles occupy non-regular sites. (For interpretation of the references to color in this figure legend, the reader is referred to the web version of this article.)

Note that the 0°-rotated and 19.1°-rotated C_{60} arrays are formed on both (Au, In)/Si(111) [44] and (Au, Tl)/Si(111) surfaces, while the 10.9°-rotated arrays occur only on the (Au, Tl)/Si(111) surface. One can see in Fig. 1a that the 19.1°-rotated array is homogeneous while the 0°-rotated and 10.9°-rotated arrays are modulated due to formation of the moiré patterns where C_{60} molecules looking brighter are arranged into the 2D lattices. In the case of the 0°-rotated array, the lattice periodicity is $\sqrt{19} \times \sqrt{19}$ in the units of the C_{60} layer lattice constant, $A = 10.02$ Å, or $\sqrt{129} \times \sqrt{129}$ in the units of the Si(111) lattice constant, $a = 3.84$ Å. It has been determined that the bright C_{60} fullerenes are those residing directly atop the Au trimers of the underlying Si(111)$\sqrt{3} \times \sqrt{3}$-Au substrate surface, while all the other molecules occupy less regular sites [44]. In the novel 10.9°-rotated array, the lattice periodicity is $\sqrt{7} \times \sqrt{7}$ in the C_{60} units and $4\sqrt{3} \times 4\sqrt{3}$ in the Si units (Fig. 2).

As shown in Ref. [38], the site atop the Au trimer occupied by the bright fullerene is the most energetically unfavorable site among all the C_{60} adsorption sites on the Si(111)$\sqrt{3} \times \sqrt{3}$-Au surface. This peculiarity appears to be the most principal feature which controls probability of C_{60} attachment to the C_{60} array periphery. In particular, in Fig. 1 one can see how this regularity controls the shape of the edge boundary of the expanding C_{60} arrays. Namely, while the edge of the featureless 19.1°-rotated array is straight, the edges of the 0°-rotated and 10.9°-rotated arrays are indented. Schematic diagram in Fig. 1b illustrates that the kink at the edge typically corresponds to the C_{60} vacant site where bright fullerene would reside according to the moiré pattern developed within the array.

In the course of island formation when random islands grown at 110 K coalesce and crystallize upon heating to RT, the same regularity

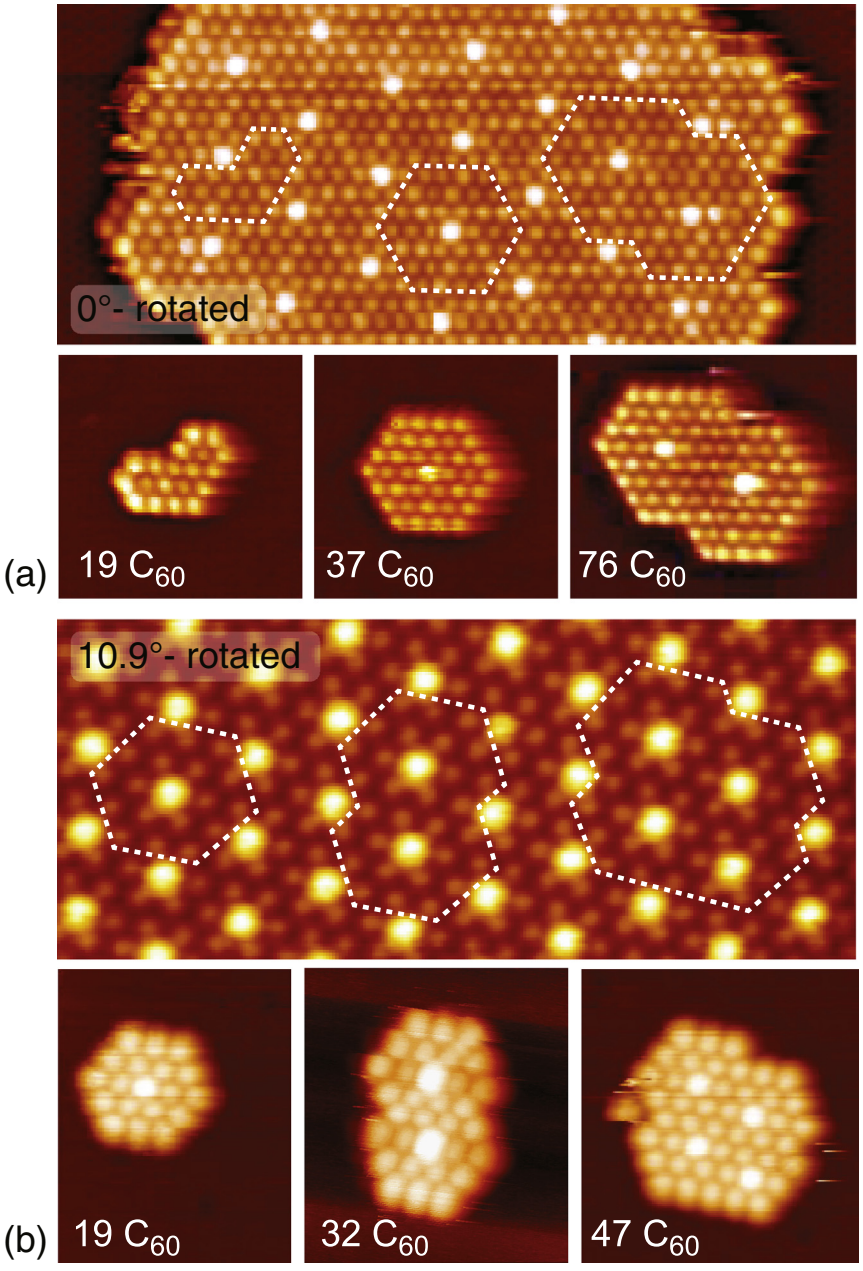

Fig. 3. Illustration disclosing the self-assembly mechanism controlling the magic island formation with (a) 0°-rotated and (b) 10.9°-rotated orientations. Magic islands shown in the lower panels are superposed on the large arrays with corresponding moiré patterns in the upper panels. The magic islands are arranged such that their borders avoid incorporating the bright fullerenes.

results in size selection and developing magic islands [38]. Namely, the magic islands adopt the shapes with minimal content of unfavorable bright fullerenes. For example, the small 0°-rotated islands containing 19 C_{60} molecules prefer non-compact boomerang shape to avoid incorporating the bright fullerene. The 0°-rotated island with 37 C_{60} molecules adopts a hexagonal shape with one bright C_{60} in the center. The islands of greater sizes have shapes of overlapped hexagons to minimize the number of bright C_{60} fullerenes. The size of the hexagons is dictated by the periodicity of the moiré pattern developing in the C_{60} array. Hence, the different moiré patterns should result in the different sets of magic islands (Fig. 3).

Fig. 3 illustrates the difference in the shapes of the 0°-rotated and 10.9°-rotated magic islands. The most vivid example is presented by the islands containing 19 C_{60} fullerenes: while the 0°-rotated 19-C_{60} island has a boomerang shape, the 10.9°-rotated island of the same size has a hexagonal shape with a bright C_{60} fullerene in the center. Note that the minimal compact 0°-rotated island having a hexagon shape contains 37 C_{60} fullerenes [38].

To elucidate which features of the surface potential relief affect the preference for particular shapes of islands, we performed molecular dynamics simulations for C_{60} island formation. As in Ref. [38], potential relief of the Si(111)$\sqrt{3}\times\sqrt{3}$-Au surface was simulated by the bell-shape (cosine function) maxima corresponding to the C_{60} adsorption sites atop Au trimers. Intermolecular C_{60}–C_{60} interaction was described by the pair interaction energy $E(r)$ calculated in [38] and approximated by the Buckingham potential. The islands of given shapes were placed on the surface and allowed to relax through changing their location and orientation until the minimal energies were reached. Typically, the energy was normalized to a single C_{60} fullerene.

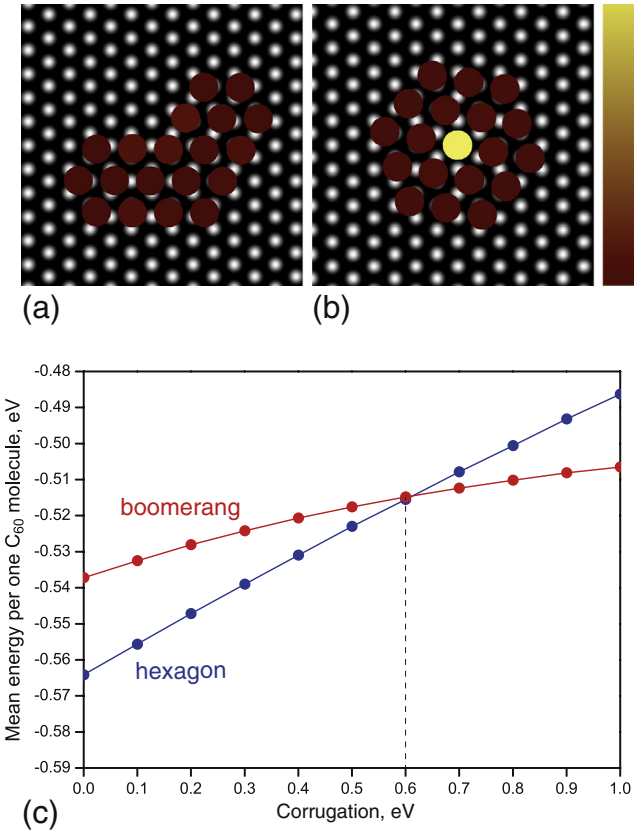

Fig. 4. Results of molecular dynamics simulations. Simulated 19-C_{60} islands having the shape of a (a) boomerang and (b) hexagon. The surface potential relief is simulated by the |*sqrt*3 $\times\sqrt{3}$ hexagonal array of the bell-shape (cosine function) maxima shown in gray scale. The adsorption energy of a given fullerene within an island is indicated by the fullerene color from the dark red-brown (for the most stable adsorption sites) to light yellow for the most energetically unfavorable sites above the potential maxima corresponding to the location of Au trimers. (c) The mean energy of the C_{60} fullerenes constituting the island as a function of the potential relief corrugation. The dependence for boomerang-shaped island is shown by a red line, that for hexagonal island by a blue line. (For interpretation of the references to color in this figure legend, the reader is referred to the web version of this article.)

Using this approach, let us consider the difference in the cluster formation in the cases of In-adsorbed and Tl-adsorbed Si(111)$\sqrt{3}\times\sqrt{3}$-Au surfaces. Remind that the 19-C_{60} island in the former case is 0°-rotated and has a boomerang shape, while in the latter case it is the 10.9°-rotated hexagonal island. As illustrated in Fig. 4, the choice of the particular island shape among the two possibilities is controlled by the corrugation amplitude of the potential relief. Namely, for the high corrugations above ~0.6 eV the boomerang-shaped island is preferable (as at In-adsorbed Au/Si(111) surface), while for the lower corrugations this is the hexagonal island (as at Tl-adsorbed Au/Si(111) surface). This tendency seems quite natural since for the low-corrugated surface the compactness of the island becomes essential factor affecting the island shape. In contrast, for the high-corrugated surface minimal number of bright C_{60} fullerenes become the dominant factor. As a consequence, the 0°-rotated C_{60} arrays would prevail there over the 10.9°-rotated, as the bright C_{60} fullerenes constitute 1/19–5% in the former and 1/7–14% in the latter. Hence, the 10.9°-rotated C_{60} arrays can occur only on the surface with the modest corrugations of the potential relief.

In principle, the In-adsorbed and Tl-adsorbed Si(111)$\sqrt{3}\times\sqrt{3}$-Au surfaces are very similar. Each contains a basic Si(111)$\sqrt{3}\times\sqrt{3}$-Au surface with a two-dimensional gas of adatoms, indium or thallium, on its top. Metal adatoms have been found to donate electrons to the metallic surface state band of the Si(111)$\sqrt{3}\times\sqrt{3}$-Au surface and for Tl this effect is greater than for In [42]. Thus, the lower corrugations of the surface potential relief for the Tl-adsorbed surface as compared to the In-modified surface can be attributed to the greater metallicity of the former surface bearing in mind that at metal surfaces molecule–substrate interaction is typically less strong than that on semiconductor surfaces.

4. Conclusions

In conclusion, studying the growth of C_{60} islands on the Tl-adsorbed Si(111)$\sqrt{3}\times\sqrt{3}$-Au surface we have found a confirmation for the universality of the recently found mechanism of self-assembled formation of the large magic islands on the surface. According to this mechanism, self-assembly is mediated by the moiré interference between an island and underlying lattice. Changing the substrate from In-adsorbed to Tl-adsorbed Si(111)$\sqrt{3}\times\sqrt{3}$-Au surface results in changing the surface potential relief to that having lower corrugations. In turn, this allows formation of the C_{60} arrays with a new orientation, where C_{60} molecular rows make an angle of 10.9° with the main crystallographic directions of Si(111) surface. These arrays demonstrate a novel moiré pattern having $\sqrt{7}\times\sqrt{7}$ periodicity which controls formation of a new set of magic islands. For example, while the 19-C_{60} magic island on the In-adsorbed Si(111)$\sqrt{3}\times\sqrt{3}$-Au surface has a boomerang shape, the island of the same size on Tl-adsorbed surface adopts a hexagonal shape. A new confirmation for the validity of the proposed self-assembly mechanism is believed to provide a promising tactic for growing large monodispersed mesoscopic structures with atomic precision.

Acknowledgments

The work was supported by the Russian Science Foundation under Grant No. 14-02-00482.

References

[1] Y.L. Wang, A.A. Saranin, A.V. Zotov, M.Y. Lai, H.H. Chang, Int. Rev. Phys. Chem. 27 (2008) 317.
[2] J. Jia, J.Z. Wang, X. Liu, Q.K. Xue, Z.Q. Li, Y. Kawazoe, S.B. Zhang, Appl. Phys. Lett. 80 (2002) 3186.

[3] V.G. Kotlyar, A.V. Zotov, A.A. Saranin, T.V. Kasyanova, M.A. Cherevik, I.V. Pisarenko, V.G. Lifshits, Phys. Rev. B 66 (2002) 165401.
[4] R.W. Li, H. Liu, J.H.G. Owen, Y. Wakayama, K. Miki, H.W. Yeom, Phys. Rev. B 76 (2007) 075418.
[5] H. Narita, A. Kimura, M. Taniguchi, M. Nakatake, T. Xie, S. Qiao, H. Namatame, Phys. Rev. B 76 (2007) 115405.
[6] H. Narita, A. Kimura, M. Taniguchi, M. Nakatake, T. Xie, S. Qiao, H. Namatame, S. Yang, L. Zhang, E.G. Wang, Phys. Rev. B 78 (2008) 115309.
[7] M.Y. Lai, Y.L. Wang, Phys. Rev. Lett. 81 (1998) 164.
[8] M.Y. Lai, Y.L. Wang, Phys. Rev. B 60 (1999) 1764.
[9] M.Y. Lai, Y.L. Wang, Phys. Rev. B 64 (2001) 241404.
[10] H.H. Chang, M.Y. Lai, J.H. Wei, C.M. Wei, Y.L. Wang, Phys. Rev. Lett. 92 (2004) 066103.
[11] Q.H. Wang, M.C. Hersam, Small 4 (2008) 915.
[12] J.L. Li, J.F. Jia, X.J. Liang, X. Liu, J.Z. Wang, Q.K. Xue, Z.Q. Li, J.S. Tse, Z. Zhang, S.B. Zhang, Phys. Rev. Lett. 88 (2002) 066101.
[13] J.F. Jia, X. Liu, J.Z. Wang, J.L. Li, X.S. Wang, Q.K. Xue, Z.Q. Li, Z. Zhang, S.B. Zhang, Phys. Rev. B 66 (2002) 165412.
[14] J.H. Byun, J.R. Ahn, W.H. Choi, P.G. Kang, H.W. Yeom, Phys. Rev. B 78 (2008) 205314.
[15] J.H. Byun, J.S. Shin, P.G. Kang, H. Jeong, H.W. Yeom, Phys. Rev. B 79 (2009) 235319.
[16] L. Vitali, M.G. Ramsey, F.P. Netzer, Phys. Rev. Lett. 83 (1999) 316.
[17] A.V. Zotov, A.A. Saranin, V.G. Kotlyar, O.A. Utas, Y.L. Wang, Surf. Sci. 600 (2006) 1936.
[18] G. Lee, C.G. Hwang, N.D. Kim, J. Chung, J.S. Kim, Phys. Rev. B 76 (2007) 245409.
[19] N.D. Kim, C.G. Hwang, J.W. Chung, Y. Kim, T.C. Kim, D.Y. Noh, K. Sumitani, H. Tajiri, O. Sakata, Surf. Sci. 602 (2008) 369.
[20] S.C. Li, J.F. Jia, R.F. Dou, Q.K. Xue, Phys. Rev. Lett. 93 (2004) 116103.
[21] S. Hu, A. Zhao, E. Kan, X. Cui, X. Zhang, F. Ming, Q. Fu, H. Xiang, J. Yang, X. Xiao, Phys. Rev. B 81 (2010) 115458.
[22] F. Ming, K. Wang, X. Zhang, J. Liu, A. Zhao, J. Yang, X. Xiao, J. Phys. Chem. C 115 (2011) 3847.
[23] N. Mariotti, C. Didiot, E.F. Schwier, C. Monney, L.E. Peret-Aebi, C. Battaglia, M.G. Garnier, P. Aebi, Surf. Sci. 606 (2012) 1755.
[24] F. Ming, G. Zhong, Q. Liu, K. Wang, Z. Zhang, X. Xiao, Phys. Rev. B 88 (2013) 125432.
[25] K. Wu, Y. Fujikawa, T. Nagao, Y. Hasegawa, K.S. Nakayama, Q.K. Xue, E.G. Wang, T. Briere, V. Kumar, Y. Kawazoe, S.B. Zhang, T. Sakurai, Phys. Rev. Lett. 91 (2003) 126101.
[26] C.G. Hwang, N.D. Kim, S.Y. Shin, J.W. Chung, J.H. Nam, M.K. Kim, C.Y. Park, J.R. Ahn, Surf. Sci. 602 (2008) 2300.
[27] J.R. Ahn, K. Yoo, J.T. Seo, J.H. Byun, H.W. Yeom, Phys. Rev. B 72 (2005) 113309.
[28] J.P. Chou, C.R. Hsing, J.C. Chen, J.Y. Lee, C.M. Wei, Surf. Sci. 616 (2013) 137.
[29] Y. Wu, Y. Zhou, C. Zhou, H. Zhan, J. Kang, J. Chem. Phys. 133 (2010) 124706.
[30] A.V. Zotov, D.V. Gruznev, O.A. Utas, V.G. Kotlyar, A.A. Saranin, Surf. Sci. 602 (2008) 391.
[31] A.A. Saranin, A.V. Zotov, O.A. Utas, V.G. Kotlyar, C.M. Wei, Y.L. Wang, Surf. Sci. 603 (2009) 2874.
[32] H. Wang, Z.Q. Zou, Appl. Phys. Lett. 88 (2006) 103115.
[33] D.Y. Wang, L.J. Chen, W. He, Q.F. Zhan, Z.H. Cheng, J. Phys. D 39 (2006) 347.
[34] J.Z. Wang, J.F. Jia, Z.H. Xiong, Q.K. Xue, Phys. Rev. B 78 (2008) 045424.
[35] D.Y. Wang, H.Y. Wu, L.J. Chen, W. He, Q.F. Zhan, Z.H. Cheng, J. Phys. Condens. Matter 18 (2006) 6357.
[36] M.A.K. Zilani, Y.Y. Sun, H. Xu, L. Liu, Y.P. Feng, X.S. Wang, A.T.S. Wee, Phys. Rev. B 72 (2005) 193402.
[37] M.A.K. Zilani, H. Xu, T. Liu, Y.Y. Sun, Y.P. Feng, X.S. Wang, A.T.S. Wee, Phys. Rev. B 73 (2006) 195415.
[38] D.V. Gruznev, A.V. Matetskiy, L.V. Bondarenko, O.A. Utas, A.V. Zotov, A.A. Saranin, J.P. Chou, C.M. Wei, M.Y. Lai, Y.L. Wang, Nat. Commun. 4 (2013) 1679.
[39] M. Yakes, M.C. Tringides, J. Phys. Chem. A 115 (2011) 7096.
[40] H.Y. Lin, Y.P. Chiu, L.W. Huang, Y.W. Chen, T.Y. Fu, C.S. Chang, T.T. Tsong, Phys. Rev. Lett. 94 (2005) 136101.
[41] H.I. Li, K.J. Franke, J.I. Pascual, L.W. Bruch, R.D. Diehl, Phys. Rev. B 80 (2009) 085415.
[42] L.V. Bondarenko, D.V. Gruznev, A.A. Yakovlev, A.Y. Tupchaya, D. Usachov, O. Vilkov, A. Fedorov, D.V. Vyalikh, S.V. Eremeev, E.V. Chulkov, A.V. Zotov, A.A. Saranin, Sci. Rep. 3 (2013) 1826.
[43] T. Nagao, S. Hasegawa, K. Tsuchie, S. Ino, C. Voges, G. Klos, H. Pfnür, M. Henzler, Phys. Rev. B 57 (1998) 10100.
[44] A.V. Matetskiy, D.V. Gruznev, A.V. Zotov, A.A. Saranin, Phys. Rev. B 83 (2011) 195421.